COBEM 2023 27TH INTERNATIONAL CONGRESS OF MECHANICAL ENGENEERING

ABCM Brazilian Society of Mechanical Sciences and Engineering
27th ABCM International Congress of Mechanical Engineering
December 04-08, 2023, Florianópolis-SC, Brazil

COB-2023-0040
BALANCING OF ROTATING SYSTEMS WITHOUT TRIAL MASSES

Diego Ataíde Couto de Paula
Kátia Lucchesi Cavalca
University of Campinas, School of Mehanical Engineering, Dept.of Integrated Systems, 200 Mendeleyev St, Campinas-SP, Brazil
d098504@dac.unicamp.br, katia@unicamp.br

Diogo Stuani Alves
University of Bath, Department of Mechanical Engineering, 4 East Cleaverton Down, BA27AY, Bath, UK
dsa41@bath.ac.uk

Abstract. *Unbalance is the most common cause of undesirable vibrations in rotating systems. Even small unbalance masses can cause high vibration amplitudes due to its quadratic relation with the rotating speed. The objective of this paper is to develop a model-based multi-plane balancing procedure for rotating machines. The proposed methodology can potentially eliminate the use of trial masses during field balancing tasks. The procedure relies on optimization techniques to find a solution that minimizes the difference between the theoretical vibrations added by noise (which represents the experimental results) and vibrations calculated numerically by the mathematical model. The rotor is supported by hydrodynamic bearings and it is modelled by the FEM. The bearings are modelled analytically by the short bearing theory. The equation of motion is solved in the frequency domain, where the Unbalance Response and optimization techniques are used to solve a Mixed-Integer Nonlinear Programming. For this class of problems, special techniques must be used to identify the unbalance. The Barrier Method is used to resolve the Nonlinear Programming. Additionally, the Outer Approximation, Branch and Bound methods, and simplex algorithms, are employed for the resulting Mixed-Integer Linear Programming. The numerical results present a striking balance identification, evidencing that the procedure adopted is indeed promising.*

Keywords: *rotating machines, balancing, unbalance identification, optimization techniques.*

1. INTRODUCTION

Rotating machines are prominent in industrial activities, especially in the power generation sector. Due to the importance of such machines, they present a great design complexity and can be composed of different rotors, couplings between shafts and between shaft and drive motor, flow seals, and hydrodynamic, magnetic or rolling element bearings. A rotating component on flexible supports that transmits power generates a series of limitations that are characteristic of several components.

In search of the highest possible degree of fidelity, mathematical models representing the causes and consequences of these delimitations have been developed to simulate the work environments of the rotating systems. In addition to the analysis of the rotor dynamic behaviour, other components of a rotating system must be considered, such as the bearings.

Hydrodynamic bearings have a thin lubricating fluid between their rigid parts in order to reduce (or eliminate) dry friction, operating temperature, and wear. Besides the understanding of the rotor characteristics, performance improvement and cost reduction are highly desirable. For these, fault detection and identification are paramount, in which the monitoring of vibrations during the operation of machines has been widely used to find out whether the operating state is acceptable over time.

Undoubtedly, unbalance is the most common cause of undesirable vibrations in rotating systems. Even small unbalance masses can cause high vibration amplitudes due to its quadratic relation with the rotating speed, which may be a significant impediment for the safe operation of the machine. Consequently, balancing is essential for any equipment.

In rotor dynamics, the traditional methods used for balancing are the influence coefficients and modal balancing. Rathbone (1929) was the forerunner of the influence coefficients method using units of motion. Bishop and Gladwell (1959) developed modal balancing, where each mode needs to be balanced and should not affect the balance of the predecessor mode. Normally, these methods need trial masses to perform balancing, which causes onerous time to add and remove masses of the equipment.

To save time, authors have been improving the methods to provide an effective balancing. Yu (2004) develops a technique to obtain the coefficients using a set of trial masses simultaneously placed to all balancing planes. Untaroiu et al. (2008) employed a convex optimization method to determinate the influence coefficients. Sudhakar and Sekhar

(2011) identified the unbalance, minimizing the equivalent forces estimated using the numerical and experimental vibrations. Knopf et al. (2015) presented an extended approach of the ISO 21940-12 standard that is adequate to reproduce exactly the vibrational behaviour in the measurement planes. The methodology shows that two residual unbalances are necessary for operating conditions outside resonance, for example, for the case of operating speeds that are usually between two critical speeds.

Yao et al. (2018) proposed two methods for identifying unbalance characteristics: the first is based on modal expansion combined with optimization algorithms for a rotating system with one disk, while the second refers to the use of applied modal expansion technique for the inverse problem for a rotor with two disks. Both the simulations and experimental results demonstrated the effectiveness of the methods. Yao et al. (2020) balanced a rotor supported by roller bearings using multiple speeds and a dual-objective optimization method.

Alves and Cavalca (2021) developed a single plane balancing method, which does not employ trial masses and can be applied a single rotating speed, to balance the first mode. Optimization methods have been developed to supply an effective balancing method to industrial applications with the goal of reducing maintenance time and consequently increasing performance.

Therefore, the present work will develop a multiplane balancing method that works without trial masses. The rotating system will be modelled by the Finite Element Method (FEM) to calculate its unbalance response. Moreover, by formulating a Mixed Integer Nonlinear Programming (MINLP) optimization, which combines methods from the Nonlinear Programming (NLP) and Mixed Integer Linear Programming (MILP) theories, one can perform the proposed balancing scheme.

2. METHODOLOGY

2.1 Model of the Rotating System by Finite Element Method

The FEM model of the rotor is represented by an assembly of the global matrices of mass, damping and stiffness, which are derived from the summation of the elementary matrices.

The equation of motion of the complete system Eq. (1) is obtained using the Lagrange equation.

$$[M]\{\ddot{q}(t)\} + ([C] + \Omega[G])\{\dot{q}(t)\} + [K]\{q(t)\} = \{f(t)\}, \quad (1)$$

where, [M], [C], [G] and [K] are respectively the global mass, damping, gyroscopic and stiffness matrices, {f(t)} is the vector of external forces and {q(t)} is the degrees of freedom vector. Additionally, the damping matrix can be calculated as proportional to the mass and stiffness matrices of the elements. Therefore:

$$[C] = \alpha[M] + \beta[K]. \quad (2)$$

However, according to Weiming and Novak (1996) and Santana (2009) the α coefficient can be neglected for steel shaft. Moreover, the foundation can be considered rigid in this work.

2.2 Hydrodynamic Bearings Model

As the journal starts to spin inside the bearing, fluid is dragged from a region of larger volume to a region of smaller volume. Such physical phenomenon is known as the wedge effect and is responsible for generating hydrodynamic pressure, which in turn sustain the applied bearing load (W_m).

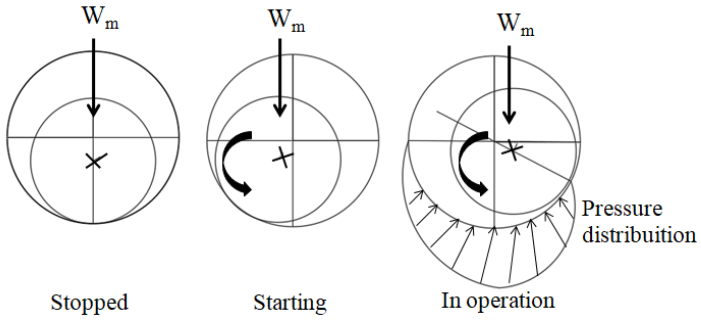

Figure 1.Working Principle of a Hydrodynamic Bearing.

One, and the most traditional, way of modelling the effects of a fluid film lubrication is through the use of the Reynolds equation. This equation was first solved analytically by Sommerfeld (1904) and Dubois and Ocvirk (1953),

who simplified the bearing as infinitely long and infinitely short, respectively. The present work adopts the short bearing theory (Krämer, 1993), which considers the pressure gradient in the circumferential direction negligible Eq. (3). Also, the bearings are represented in the rotating system by linear stiffness and damping coefficients. It is important to point that in frequency range of analysis, the short bearing analytical approach gives similar results than numerical solution of a finite bearing.

$$\frac{\partial}{\partial x}\left[h^3\frac{\partial p}{\partial x}\right] = 6\mu\left(V\frac{\partial h}{\partial \theta}\right), \tag{3}$$

where, p is the pressure, x, θ and z are, respectively, the axial, circumferential and vertical coordinates, h is the thickness of the lubricant film:

$$h = C_R + y\sin(\theta) + z\cos(\theta), \tag{4}$$

C_R is the radial clearance of the bearing, V is the journal linear velocity, and μ is the lubricant viscosity.

Thus, considering the simplifications proposed by Dubois and Ocvirk (1953), the pressure distribution can be computed as present in Eq. (5).

$$\mathrm{p}\,(\theta, \mathrm{x}) = \frac{3\varepsilon\mu\sin(\theta)}{\mathrm{R_m C_R}^2(1+\varepsilon\cos(\theta))^3}\left(\frac{\mathrm{L_m}^2}{4} - \mathrm{x}^2\right) + \mathrm{pa}, \tag{5}$$

where: R_m and L_m are the radius and length of the bearing, respectively, and ε is the dimensionless eccentricity.

By integrating the pressure distribution over the inner surface of the bearing, one can obtain the hydrodynamic forces in the tangential and radial direction:

$$\mathrm{F_t} = \frac{\mu\Omega\mathrm{RL}^3}{\mathrm{C_R}^2}\left(\frac{\pi\varepsilon}{4(1-\varepsilon^2)^{3/2}}\right);\ \mathrm{F_r} = \frac{\mu\Omega\mathrm{RL}^3}{\mathrm{C_R}^2}\left(\frac{\varepsilon^2}{(1-\varepsilon^2)^2}\right). \tag{6}$$

Finally, the derivatives of the hydrodynamic forces with respect to the position and velocity of the centre of the journal give the linear stiffness and damping coefficients presented in Eq. (7), Krämer (1993).

$$\frac{\partial F_i}{\partial x_k} = k_{ik} = \gamma_{ik}\frac{W}{C_R};\ \ \frac{\partial F_i}{\partial \dot{x}_k} = d_{ik} = \beta_{ik}\frac{W}{C_R\Omega}, \tag{7}$$

The following auxiliary variables are used to calculate the equivalent coefficients, Krämer (1993):

$$\gamma_{11} = [2\pi^2 + (16-\pi^2)\varepsilon^2]A(\varepsilon);\ \gamma_{12} = \frac{\pi}{4}\frac{\pi^2 - 2\pi^2\varepsilon^2 - (16-\pi^2)\varepsilon^4}{\varepsilon(1-\varepsilon^2)^{\frac{1}{2}}}A(\varepsilon); \tag{8}$$

$$\gamma_{21} = -\frac{\pi}{4}\frac{\pi^2 + (32+\pi^2)\varepsilon^2 + (32-2\pi^2)\varepsilon^4}{\varepsilon(1-\varepsilon^2)^{\frac{1}{2}}}A(\varepsilon);\ \gamma_{22} = \frac{\pi^2 + (32+\pi^2)\varepsilon^2 + (32-2\pi^2)\varepsilon^4}{1-\varepsilon^2}A(\varepsilon);$$

$$\beta_{11} = \frac{\pi}{2}\frac{(1-\varepsilon^2)^{1/2}}{\varepsilon}[\pi^{2+}(2\pi^2-16)\varepsilon^2]\mathrm{A}(\varepsilon);\ \beta_{12} = \beta_{21} = -[2\pi^{2+}(4\pi^2-32)\varepsilon^2]\mathrm{A}(\varepsilon);$$

$$\beta_{22} = -\frac{\pi}{2}\frac{\pi^2+(48-2\pi^2)\varepsilon^2+\pi^2\varepsilon^4}{\varepsilon(1-\varepsilon^2)^{\frac{1}{2}}}\mathrm{A}(\varepsilon);\ \mathrm{A}(\varepsilon) = \frac{4}{[\pi^2+(16-\pi^2)\varepsilon^2]^{3/2}}.$$

2.3 Solution of the Equation of Motion in the Frequency Domain

The solution of the equation of motion in the frequency domain is used for the calculation of the unbalance parameters. Starting from Eq. (1), it is possible to consider that the displacement vector of the system **q**(t) and the excitation forces **f**(t) have an oscillatory behaviour, that is:

$$\{q(t)\} = \{q_0\}e^{jwt}. \tag{9}$$

$$\{f(t)\} = \{f_0\}e^{j(wt+\delta)} = \{f_0\}(e^{jwt}e^{j\delta}). \tag{10}$$

where $\{q_0\}$ is the amplitude of the system, and $\{f_0\}$ and δ are the amplitudes and phases of the excitation forces, respectively.

Substituting the first and second derivatives of **q**(t), with respect to time, in Eq. (1), one obtains the equation of motion in the frequency domain.

$$\left(-\Omega^2[M] + \ j\Omega([C] + \ \Omega[G]) + \ [K]\right)\{q_0\} = \{f_0\}e^{j\,\delta}, \tag{11}$$

which is a system of linear equations.

2.4 Balancing Procedure

The balancing strategy proposed in this work is based on a model-based identification of the unbalance parameters - namely the unbalance moment mass × eccentricity (me), phase angle (δ), balancing planes (x) - as initially developed by Alves and Cavalca (2021) To achieve this goal, it is necessary to minimize the difference between the vibrations coming from a physical system and from the mathematical model of that system, in which the unbalance parameters are the optimization variables. Therefore, using the least squares technique, it is possible to write an appropriate objective function for the problem:

$$f(\boldsymbol{\chi}) = \frac{1}{2}\|\boldsymbol{q}(\,me, \delta, x) - \bar{\boldsymbol{q}}\|_2^2, \tag{12}$$

where, $\{\bar{q}\}$ is the vibration amplitude added by noise (which will emulate the behaviour of the physical system), and $\{\chi\}$ is the vector with the unbalance parameters.

In this way, the identification of the unbalance becomes a problem that search to minimize the difference between the theoretical vibrations and the theoretical vibrations added by noise, and can be shown mathematically as:

$$\begin{cases} min \rightarrow f(\boldsymbol{\chi}) = \dfrac{1}{2}\|\boldsymbol{q}(\boldsymbol{\chi}) - \bar{\boldsymbol{q}}\|_2^2 \\ \quad s.a\,.0 \ \leq me_{nd} \ \leq me_{max} \quad nd = 1, \ldots, p \\ \qquad 0 \leq \delta_{\,nd} \ \leq 2\pi \\ \qquad\ 0 \leq x_{nd} \ \leq L_r \end{cases} \tag{13}$$

where, $me_{\max}$ is the maximum value imposed for the unbalance moment, L_r is the rotor length and nd represents the p-th unbalance acting on the system.

However, since the FEM was used as the modelling technique, the unbalance planes can only be associated with the nodes of the discrete rotating system. This fact adds an extra layer of complexity to the identification process, forcing one of the variables to be discrete in nature.

When some of variables are integer and the objective function and/or constraints are constituted by non-linear functions, one has a Mixed-Integer Nonlinear Programming (MINLP). To solve this class of optimization problem, special techniques must be used.

One of those techniques is the Outer Approximation. This technique solves the MINLP through the solution of a sequence of Mixed-Integer Linear Programming (MILP) and Nonlinear Programming (NLP) problems. The MILP is obtained by introducing an auxiliary variable η (greater than or equal to the value of the original objective function) and linearizing the objective and constraint functions following the principles of linearization (Lee and Leyffer 2012). On the other hand, the NLP is created by fixing values for the integer variables calculated via the previous MILP. Only the continuous variables must be found during the NLP. Thus, the solution of the NLP subproblem is added to the MILP in the form of a new constraint function that enables the computation of new values for the integer variables, which in turn will develop a new NLP subproblem. This process is repeated until the MILP generates no feasible solution. For more details of the method see Alves and Cavalca (2021), Lee and Leyffer (2012) and Luenberger (2008). Using this tactic, it is possible to rewrite the optimization problem previously formulated in Eq. (13):

$$\begin{cases} \min \rightarrow \eta \\ s.a.\ f\left(\boldsymbol{\chi}^{(\mathrm{i})}\right) + \boldsymbol{\nabla f}\left(\boldsymbol{\chi}^{(\mathrm{i})}\right)^{\mathrm{T}}\left(\boldsymbol{\chi} - \boldsymbol{\chi}^{(\mathrm{i})}\right) \leq \eta, \forall \boldsymbol{\chi}^{(\mathrm{i})} \in K \\ 0 \leq me_{nd} \leq me_{max} \\ 0 \leq \delta_{nd} \leq 2\pi nd = 1, \ldots, p \\ 0 \leq x_{nd} \leq L_r \\ x = \sum_{j=1}^{nn} z_j\ coord(j) \\ z_j \leq 1, j = 1, \ldots., nnodes \\ \sum_{j=1}^{nodes} z_j = 1, \mathrm{z} \in [0\ 1] \end{cases} . \tag{14}$$

where, $\boldsymbol{\nabla f}(\boldsymbol{\chi})$ is the gradient of the objective function $f(\boldsymbol{\chi})$, nnodes is the total quantity of nodes of the rotating system and coord is the vector containing the coordinates of the nodes.

The solution of the NLP must guarantee the global minimum for the corrected unbalance identification. In order to assure such requirement, the Matlab® GlobalSearch function is used (Ugray et al. 2007). The solver attempts to find a solution that has the lowest objective function value. For this purpose, the solver is designed to search in more than one basin of attraction through the generation of several starting points. The minimization is then accomplished using the Barrier Method, BFGS quasi-Newton (Broyden, Fletcher, Goldfarb and Shanno 1970) and Wolf conditions (Nocedal 1999) for several of those starting points.

If an objective function f(**x**) is smooth, the vector –∇**f**(**x**) points to the direction where f(**x**) decreases most quickly. The equation of the steepest descent,

$$\frac{d\boldsymbol{x}(t)}{dt} = -\nabla \mathbf{f}(\mathbf{x}(\mathrm{t})), \tag{15}$$

yields a path x(t) that goes to a local minimum as t increases. Generally, initial values $\mathbf{x}_0$ that are close to each other present steepest descent paths that tends to the same minimum point. A basin of attraction is the set of initial values leading to the same local minimum. To exemplify this process, Figure 2 shows two one-dimensional minima and different basins of attraction. The arrows show the directions of the steepest descent, and the black dots represent a local minimum. Every steepest descent path, starting at a point $\mathbf{x}_0$, goes to the black dot in the basin containing $\mathbf{x}_0$.

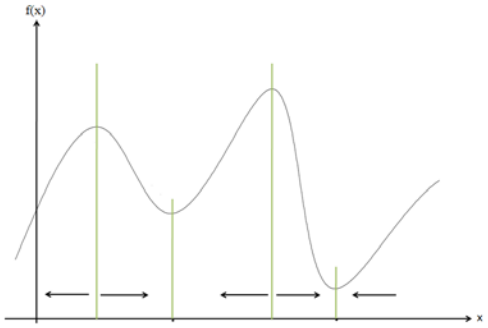

Figure 2. Basin of Attraction.

3. NUMERICAL RESULTS

A rotating system composed of three disks is modelled (Figure 3 and Table 1) to assess the unbalance identification. For this system, several cases are simulated, and the effectiveness of the balancing procedure is verified. The choice for the analysed cases was made in the following way: unbalance masses can be inserted in the left or right face of Disks 1, 2, and 3. Therefore, eight cases can be generated by combination process. Additionally, to emulate the experimental signal, white gaussian noise (with a noise to signal ratio of 40%) was added to the results of the aforementioned simulated cases.

The rotor is composed of a steel shaft, which properties are E = 200 GPa and ρ = 7850 kg/m^3, with a length of 1021 mm and a diameter of 13 mm. It is subdivided into 22 cylindrical beam elements, three steel disk elements located at nodes 7, 12 and 17, and it is supported by two identical hydrodynamic bearings (Table 2) located at nodes 2 and 22. The oil film viscosity is adopted constant. The sources of external excitation are rotating unbalances located at nodes

referent to the faces of the disks. Unbalance masses weighting m=3.2 g and with an eccentricity of 37 mm in relation to the centre of the disk were considered for all disks. The stiffness proportionality coefficient was adopted as $\beta = 1.0 \times 10^{-4}$.

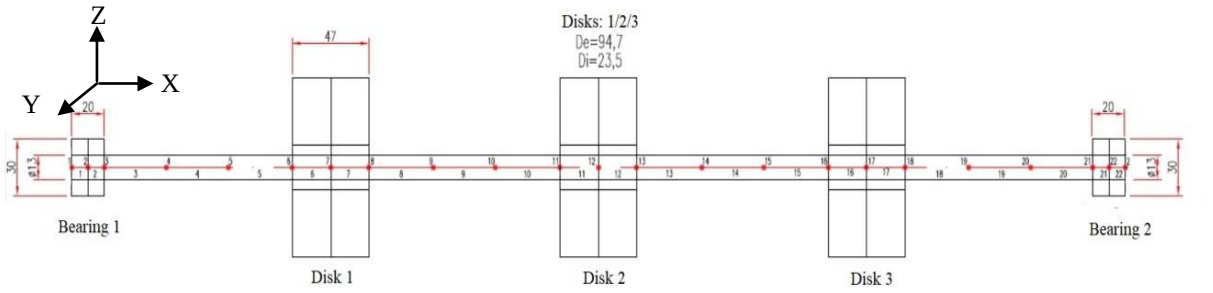

Figure 3. FEM model of the simulated rotor.

Table 1. Details of the rotating system model.

Element Number	Element Type	Internal diameter [mm]	External Diameter [mm]	Lenght [mm]
1, 2, 21, 22	Beam	0	30	10
3, 4, 5, 8, 9, 10,13, 14, 15, 18, 19, 20	Beam	0	13	70
6, 7, 11, 12, 16, 17	Beam	0	23,5	23,5
23, 24, 25	Disk	23,5	94,7	47

Table 2. Bearings parameters.

Bearing Diameter (D)	30 mm
Bearing Lenght (L)	20mm
Bearing radial clearance (C_R)	90μm
Lubricant Viscosity (μ)	51mPa.s

Figure 4 presents the unbalance response for the rotating system described. It is possible to observe that the first three critical speeds are approximately at 57, 231 and 510 rad/s. For this simulation the phases of the unbalance masses were at 135° at disk 1, 225° at disk 2, and 45° at disk 3, with respect to the 0° of the trigonometric circle.

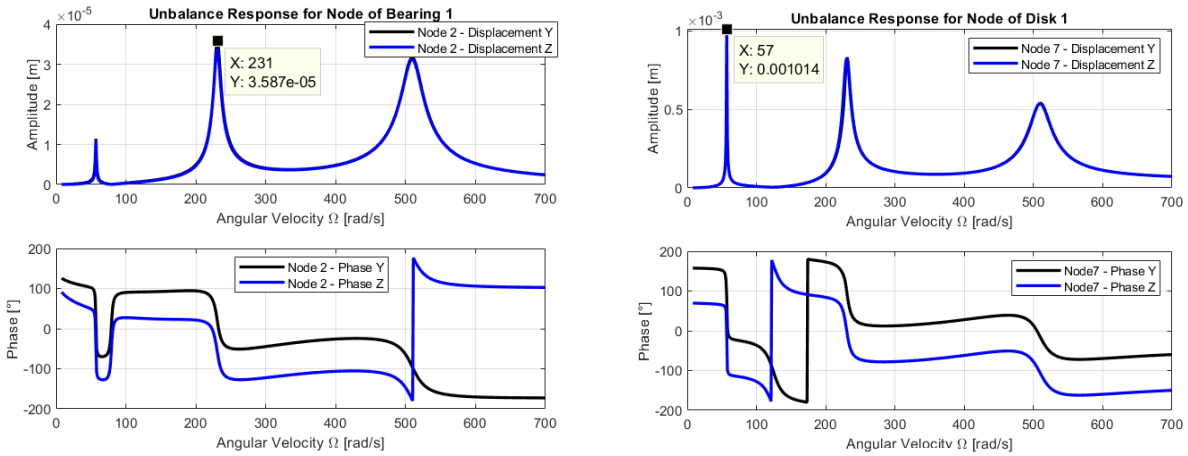

(a) (b)

Figure 4. Unbalance Response. (a)Bearing 1 (node 2), (b) Disk 1 (node 7).

The displacement vector utilized in the objective function is composed of all vibration information (vertical and horizontal complex vibration) related to the first three critical speeds at the bearings position. As shown in Table 3, the

algorithm was able to correctly identify all cases, the greatest error (0.541%) being found for the third disk unbalance mass for the 6-13-18 case.

However, it is known that for hydrodynamic bearings the average fluid velocity is approximately half of the shaft rotating speed. This fact causes the well-known fluid induced instability when the shaft reaches a rotating speed approximately twice the first critical speed. In this situation the rotor becomes unstable, and any further operating speed becomes impossible to reach. Then, the operational range of this rotor is up to around 114 rad/s. Therefore, in an experimental analysis it would not be possible to work with the second and third critical speeds, as they are above the instability threshold. Thus, it is necessary to select a different set of rotating speeds to construct the displacement vector.

Rigid rotors work below the first critical speed and consequently are balanced at a single rotational speed (ISO 21940-11). On the other hand, flexible rotors working above the first critical speed need to be balanced at various rotational speeds according to ISO 21940-12. In the latter case the rotor is successively balanced on a modal basis at a series of balancing speeds, one at a time. In other words, each mode excited by its respective critical speed is balanced from the slowest to the fastest balancing speed, which can be selected close to resonances if within the rotor operating range. The ISO 21940-12 standard does not provide any information regarding rotors significantly influenced by the third mode.

Table 3. Values and errors for nodes combination 6-11-16, 8-13-18, 6-11-18 e 6-13-16, 6-13-18, 8-11-16, 8-11-18 e 8-13-16 for awgn-40.

	Expected	Nodes 6-11-16	Error nodes 6-11-16	Nodes 8-13-18	Error nodes 8-13-18	Nodes 6-11-18	Error nodes 6-11-18	Nodes 6-13-16	Error nodes 6-13-16
Me01	0,0001184	0,0001183	-0,051%	0,0001184	0,000%	0,0001183	-0,110%	0,0001184	-0,042%
Phase01	2,3562	2,3561	-0,004%	2,3567	0,021%	2,3582	0,085%	2,356	-0,008%
Node1	6/8	6	0,000%	8	0,000%	6	0,000%	6	0,000%
Me02	0,0001184	0,0001183	-0,051%	0,0001183	-0,051%	0,0001183	-0,059%	0,0001183	-0,059%
Phase02	3,927	3,9243	-0,069%	3,9241	-0,074%	3,9252	-0,046%	3,9246	-0,061%
Node02	11/13	11	0,000%	13	0,000%	11	0,000%	13	0,000%
Me03	0,0001184	0,0001182	-0,203%	0,0001183	-0,110%	0,0001184	-0,025%	0,0001182	-0,203%
Phase03	0,7854	0,7852	-0,025%	0,7851	-0,038%	0,7827	-0,344%	0,785	-0,051%
Node3	16/18	16	0,000%	18	0,000%	18	0,000%	16	0,000%
	Expected	Nodes 6-13-18	Error nodes 6-13-18	Nodes 8-11-16	Error nodes 8-11-16	Nodes 8-11-18	Error nodes 8-11-18	Nodes 8-13-16	Error nodes 8-13-16
Me01	0,0001184	0,0001180	-0,296%	0,0001182	-0,160%	0,0001182	-0,203%	0,0001183	-0,076%
Phase01	2,3562	2,3555	-0,030%	2,361	0,204%	2,3558	-0,017%	2,357	0,034%
Node1	6/8	6	0,000%	8	0,000%	8	0,000%	8	0,000%
Me02	0,0001184	0,0001181	-0,287%	0,0001182	-0,211%	0,0001183	-0,076%	0,0001183	-0,068%
Phase02	3,927	3,9277	0,018%	3,9229	-0,104%	3,9276	0,015%	3,9274	0,010%
Node02	11/13	13	0,000%	11	0,000%	11	0,000%	13	0,000%
Me03	0,0001184	0,0001178	-0,541%	0,0001183	-0,110%	0,0001181	-0,228%	0,0001183	-0,051%
Phase03	0,7854	0,7825	-0,369%	0,7828	-0,331%	0,7837	-0,216%	0,7847	-0,089%
Node3	16/18	18	0,000%	16	0,000%	18	0,000%	16	0,000%

So, the new rotating speeds selected for the balancing procedure considers the ISO 21940-12 standard recommendations. In addition to those, several combinations of balancing speeds were tested, and the set that produced the lowest objective function value was used as the ultimate set. Therefore, the new balancing speeds chosen are 30, 57, 90 and 110 rad/s.

When the previous balancing speeds are selected, the first critical speed was properly balanced with a vibration reduction of 99.45% at Bearing 1 and 99 .88% at Disk1. The vibrations at second critical speed (231 rad/s) presented a reduction of 75.12% for Bearing 1 and 76.16% for Disk 1. Finally, the displacement amplitudes of the third critical speed (510 rad/s) are reduced by 7.15% and 11.93% in bearing 1 and disk 1, respectively. This trend can be observed in Figures 5 and 6 for the 6-11-16 case.

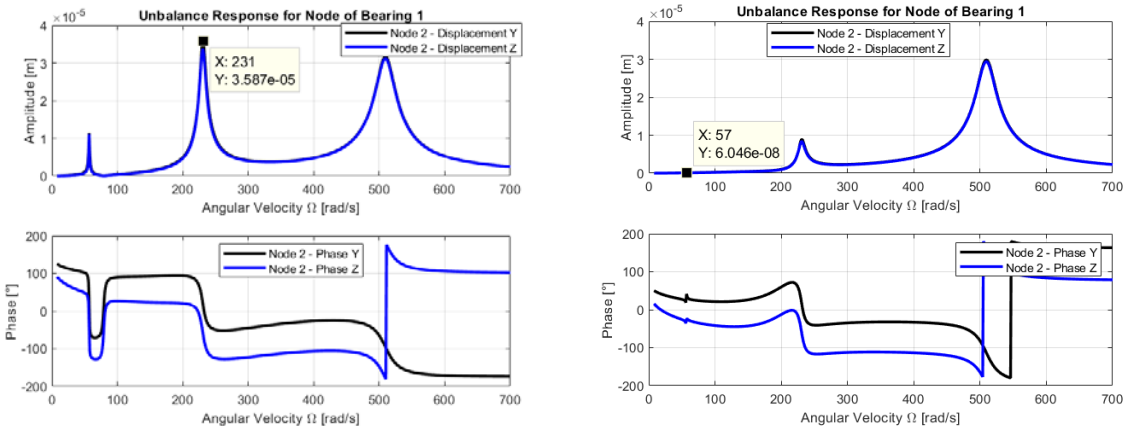

(a) (b)

Figure 5: Unbalance Response of Bearing 1 (node 2) nodes 6-11-16. (a) unbalanced system, (b) balanced system.

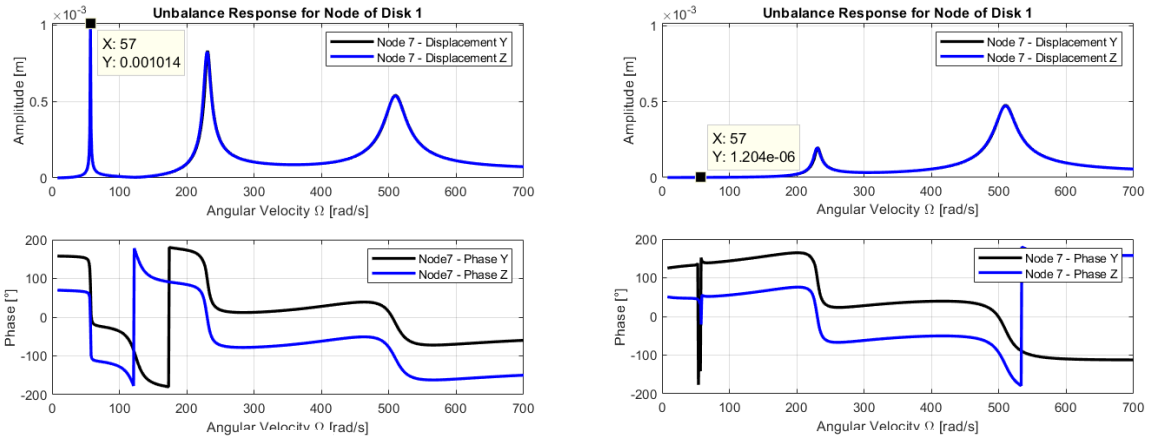

(a) (b)

Figure 6: Unbalance Response of Disk 1 (node 7) nodes 6-11-16. (a) unbalanced system, (b) balanced system.

It is well known that unbalance is distributed all over the length of a rotor. Therefore, the unbalance can sometimes be located outside the disks' region. To simulate such condition, unbalance masses were added to nodes 9, 10 and 15, as presented in Table 4. Again, because of the fluid induced instability, the balancing speeds 30, 57, 90 and 110 rad/s are used for the identification procedure.

Table 4. Unbalance parameters added at nodes 9, 10 e 15.

Imposed Unbalance Parameters				Values found			
Me01	$1{,}184 \times 10^{-4}$	Node2	10	Me01	$1{,}04 \times 10^{-4}$	Node2	11
Phase01	2,3562	Me03	$1{,}184 \times 10^{-4}$	Phase01	2,9269	Me03	$1{,}08 \times 10^{-4}$
Node1	9	Phase03	0,7854	Node1	6	Phase03	0,6988
Me02	$1{,}184 \times 10^{-4}$	node3	15	Me02	$6{,}70 \times 10^{-5}$	node3	18
Phase02	3,927			Phase02	3,1726		

The outcome of the optimization problem is also shown in Tab. 4, and the balancing of the system using the identified parameters can be seen in Figures 7 and 8. It is interesting to note that, again the first critical speed was effectively balanced, presenting a vibration reduction of 99.84% at Bearing 1 and 99.78% atDisk1. The amplitude of the second critical speed was reduced 74.42% at Bearing 1 and 74.70% at Disk 1. Lastly, for the third critical speed on observes a displacement reduction of 11.37% (Figure 7) and 24.07% for Bearing 1 and Disk 1 (Figure 8), respectively.

So, by analysing the results presented, the developed procedure was efficient in performing theoretical balancing of rotors. By selecting rotating speeds near the critical speeds of the system, the results gradually improve, with a greater

vibration reduction. Since no selected balancing speed is close enough to the third critical speed, the balancing for this region is not very effective. However, it is important to highlight that this rotating system will not operate above 140 rad/s. Additionally, it is worth noting that the proposed balancing model was effective in all cases analysed and showed good convergence, showing that the method is promising.

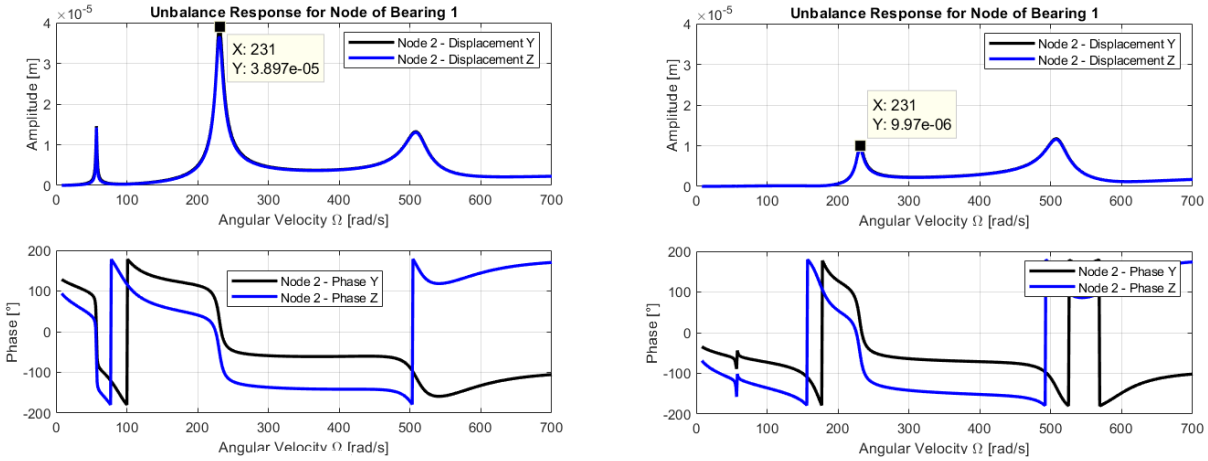

(a) (b)

Figure 7. Unbalance Response of Bearing 1 (node 2) – Nodes 9-10-15. (a) unbalanced system, (b) balanced system

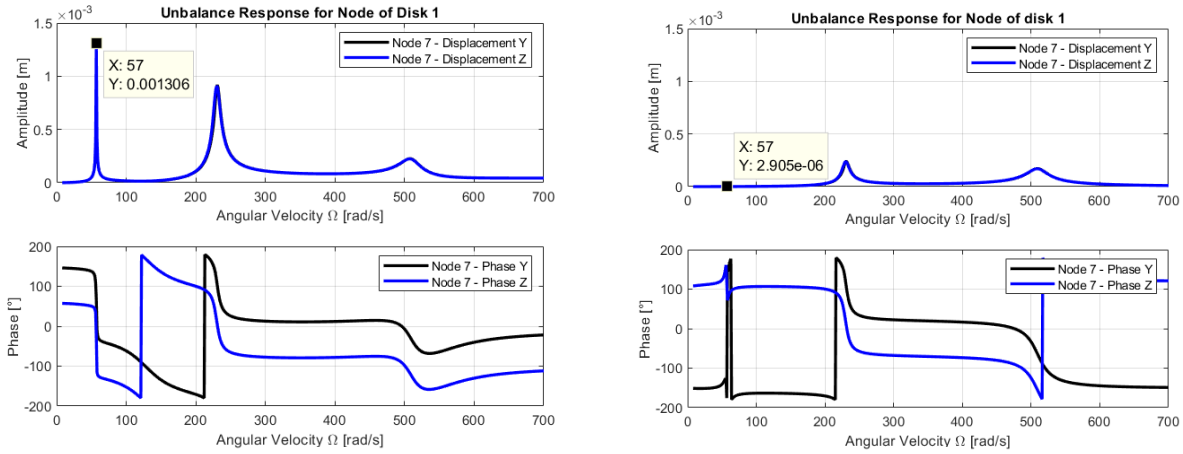

(a) (b)

Figure 8. Unbalance Response of Disk 1 (node 7) - Nodes 9-10-15. (a) unbalanced system, (b) balanced system.

4. CONCLUSIONS

The multi-plane balancing method developed shown to be able to theoretically balance a rotating system supported by hydrodynamic bearings without the need for trial masses. It presents good convergence and the errors found are acceptably small, evidencing that the method is promising.

The use of specific critical speeds to construct the complex vibrations vector used in the objective function is essential for the calculation of the unbalance parameters, demonstrating that modal analysis combined with the least squares method is effective for the optimization process.

Hydrodynamic bearings operating speed range are limited due to the fluid induced instability, which can affect the effectiveness of the theoretical balancing, since not all rotating speeds can be selected for balancing purposes. However, following the ISO 21940-12 standard guidelines, it was possible to successfully carry out the theoretical balancing.

5. REFERENCES

ALVES, D. S.; CAVALCA, K. L. Investigation into the influence of bearings nonlinear forces in unbalance identification. Journal of Sound and Vibration, v. 492, p. 115807, 2021.

BAZARAA, M. S.; SHERALI, H. D.; SHETTY, C. M. Nonlinear Programming – Theory and Algorithms. Jhon Wiley & Sons, New Jersey, 2006.

BISHOP, R. E. D.; GLADWELL, G. M. L. The Vibration and Balancing of an Unbalanced Flexible Rotor. Journal of Mechanical Engineering Science, v.1, n.1, p. 66-77, 1959.

BROYDEN, C.G. The Convergence of a Class of Double-rank Minimization Algorithms. J. Inst. Maths. Applics, v. 6, p. 76–90, 1970.

DUBOIS, C. B.; OCVIRK, FW," Analytical Derivation and Experimental Evaluation of Short-Bearing Approximation for Full Journal Bearing3," Report 1157. Nation Advisory Committee for Aeronautics, 1953.

FLETCHER, R. A new approach to variable metric algorithms. The computer journal, v. 13, n. 3, p. 317-322, 1970.

GOLDFARB, Donald. A family of variable-metric methods derived by variational means. Mathematics of computation, v. 24, n. 109, p. 23-26, 1970.

INTERNATIONAL STANDARD. ISO 21940-11: Mechanical vibration – Rotor Balancing – Part 11: Procedures and tolerances for rotors with rigid behaviour. Geneva, 2016. 28p.

INTERNATIONAL STANDARD. ISO 21940-12: Mechanical vibration – Rotor Balancing – Part 12: Procedures and tolerances for rotors with flexible behaviour. Geneva, 2016. 42p.

KNOPF, E.; KRÜGER, T.; NORDMANN, R.. Residual unbalance determination for flexible rotors at operational speed. In: Proceedings of the 9th IFToMM International Conference on Rotor Dynamics. Springer International Publishing, 2015. p. 757-768.

KRÄMER, E., “Dynamics of rotors and foundations”, Springer-Verlag, New York, 381p., 1993.

LEE, J., LEYFFER, S. Mixed Integer Nonlinear Programming. In: The IMA Volumes in Mathematics and its Applications, v. 154, Springer, New York, 2012.

LUENBERGER, D. G.; YE, Y., “Linear and Nonlinear Programing”, Springer Science+Business Media LLC, New York, 2008.

Mathworks Help Center. Acessoem 8 de setembro de 2022. URL: https://www.mathworks.com/help/gads/what-is-global-optimization.html#bsbalkx-1.

NELSON, H. D., McVAUGH, J. M., The dynamics of rotor-bearing systems using finite elements. ASME Journal of Engineering for Industry, v. 98, n. 2, p. 593-600, 1976.

NELSON, H. D., A finite rotating shaft element using timoshenko beam theory. ASME Journal of Mechanical Design, v. 102, n. 4, p. 793-803, 1980.

NOCEDAL, J., Wright, S. J., Numerical Optimization. Springer-Verlag, New York, 1999.

SHANNO, David F. Conditioning of quasi-Newton methods for function minimization. Mathematics of computation, v. 24, n. 111, p. 647-656, 1970.

SOMMERFELD, A., “ZurHydrodynamischenTheorie der Schmiermittelreibung”, Zs. Math. And Phys, v. 50, p. 97–155, 1904.

SUDHAKAR, G. N. D. S.; SEKHAR, A. S. Identification of unbalance in a rotor bearing system. Journal of Sound and Vibration, v. 330, n. 10, p. 2299-2313, 2011.

RATHBONE, T. C., “Turbine Vibration and Balancing”, Trans. of American Society of Mechanical Engineers, Vol. 51, Part I, p. 267-284, 1929.

UGRAY, Z.; LASDON, L.; PLUMMER. J. C.; GLOVER, F.; KELLY, J.; MARTÍ, R. Scatter search and local NLP solvers: A multistart framework for global optimization. INFORMS Journal on computing, v. 19, n. 3, p. 328-340, 2007.

UNTAROIU, C. D.; ALLAIRE, Paul E.; FOILES, William C. Balancing of flexible rotors using convex optimization techniques: optimum min-max LMI influence coefficient balancing. Journal of Vibration and Acoustics, v. 130, n. 2, 2008.

WEIMING, L.; NOVAK, M. Dynamic behaviour of turbine-generator-foundation systems. Earthquake Engineering & Structural Dynamics, v. 24, n. 3, p. 339-360, 1996.

YAO, J.; LIU, L.; YANG, F.; SCARPA, F.; & GAO, J. Identification and optimization of unbalance parameters in rotor-bearing systems. Journal of Sound and Vibration, v. 431, p. 54-69, 2018.

YAO, J.; YANG, F.; SU, Y.; SCARPA, F.; & Gao, J. Balancing optimization of a multiple speeds flexible rotor. Journal of Sound and Vibration, v. 480, p. 115405, 2020.

YU, X. General influence coefficient algorithm in balancing of rotating machinery. International Journal of Rotating Machinery, v. 10, n. 2, p. 85-90, 2004.

6. RESPONSIBILITY NOTICE

The authors are the only responsible for the printed material included in this paper.